Journal of Energy Chemistry 60 (2021) 222–228

Contents lists available at ScienceDirect

Journal of Energy Chemistry

journal homepage: www.elsevier.com/locate/jechem

http://www.journals.elsevier.com/journal-of-energy-chemistry/

The effect of electrochemically inactive Ti substituted for Ru in $Li_2Ru_{1-x}Ti_xO_3$ on structure and electrochemical performance

Ye Yao [a], Lu Zhang [b], Florian Sigel [c], Björn Schwarz [c,*], Helmut Ehrenberg [c], Gang Chen [b], Fei Du [b,*], Chunzhong Wang [b]

[a] Changchun Normal University, Changchun 130031, Jilin, China
[b] Key Laboratory of Physics and Technology for Advanced Batteries (Ministry of Education), State Key Laboratory of Superhard Materials, College of Physics, Jilin University, Changchun 130012, Jilin, China
[c] Institute for Applied Materials (IAM), Karlsruhe Institute of Technology (KIT), 76344 Eggenstein-Leopoldshafen, Germany

ARTICLE INFO

Article history:
Received 13 November 2020
Revised 22 December 2020
Accepted 31 December 2020
Available online 14 January 2021

Keywords:
$Li_2Ru_{1-x}Ti_xO_3$
Lithium ion batteries
Inactive element substitution
XRD
NMR

ABSTRACT

The approach of substituting electrochemically active with inactive elements has widely been used to improve the electrochemical performance of Li-rich intercalation cathode materials. This especially is true for Li-rich compounds where almost all of the Li^+ ions are reversibly (de)intercalated during electrochemical cycling. The beneficial mechanism behind this substitution with electrochemically inactive elements is still not clear yet. Li_2RuO_3 is chosen as basis for a model solid solution system to investigate the effect of electrochemically inactive elements owing to its high specific capacity of more than 300 mAh g^{-1} and the significant contribution of anion redox mechanism. Herein, $Li_2Ru_{1-x}Ti_xO_3$ solid solution series are synthesized and the effect of substituting with electrochemical inactive Ti for Ru on structure and electrochemical performance have been comprehensively investigated. The electrochemical performance is significantly improved, especially for $Li_2Ru_{0.8}Ti_{0.2}O_3$, and the capacity retention after 50 cycles increases from 81% to 90%, as compared to the end member Li_2RuO_3. Results of electrochemical impedance spectroscopy show that Ti substitution reduces the charge transfer impedance, which favors the Li^+ diffusion across the electrolyte–electrode interface and improves the electronic conductivity. For the first time, nuclear magnetic resonance was utilized to confirm that a small part of Ti ions exchange their position with Li ions in the Li layer. This research provides a better understanding of electrochemical inactive element substitution and strong insights for the functional design of the next generation of Li-rich cathode materials.

1. Introduction

Lithium ion batteries (LIBs) have contributed greatly to the human society over the past 30 years. They are used in electric vehicles, portable electronic devices, and many other applications as energy storage systems [1–5]. With the rapid development of 3C (computer, cellphone and camera) products and electric vehicles, there is a growing demand for high-performance batteries with higher energy and power densities. Therefore, the exploitation of high capacity electrode materials remains in high demand [6–9]. In essence, the energy density of LIBs depends on the capacity of cathode and anode materials and their potential differences. At present, carbon materials have become the first choice of negative electrode materials for commercial batteries because of their low cost and excellent performance. For example, the theoretical capacity of graphite can reach 372 mAh g^{-1}, and the specific capacity of 360 mAh g^{-1} can be obtained in practical applications [10–12]. However, the highest capacity of the widely used layered oxide cathode is still ≈ 200 mAh g^{-1} ($LiNi_{1/3}Co_{1/3}Mn_{1/3}O_2$) [13–16]. Therefore, searching for cathode material with high capacity and high voltage to match the anode material is key to improving the energy density of LIBs.

For conventional cathode active materials, such as $LiMO_2$ (M = transition metal), lithium storage capacities depend solely on the cationic redox reactions. However, this restriction was overcome by Li-rich layered compounds among others as revealed by comprehensive research activities during the past decades [17–19]. The anionic redox contribution by oxygen has been accepted as an effective way to promote the capacity of the layered

* Corresponding authors.
E-mail addresses: bjoern.schwarz@kit.edu (B. Schwarz), dufei@jlu.edu.cn (F. Du).

https://doi.org/10.1016/j.jechem.2020.12.037

oxide cathodes for LIBs. Among numerous cathode materials with anionic redox reaction mechanism, Li_2RuO_3 has attracted worldwide attention recently owing to its high specific capacity of more than 300 mAh g^{-1} [20–23]. Ru ions can provide more electrons that participate in the electrochemical process, because Ru^{5+} is available compared with Mn-based Li-rich compound where the oxidation state is restricted to Mn^{4+}. Moreover, Ru ions play a crucial role in stabilizing the anion redox reaction and Ru-based Li-rich compounds show a much more stable reversible oxygen redox process and are structurally more stable than Mn-based Li-rich compounds. Ru is a noble and expensive metal and surely Ru-based cathode materials have only little prospect of being commercially implemented as cathode material for LIBs. Still the deeper understanding of the mechanism underlying these Ru-based Li-rich compounds that serve as a kind of model system will help to design and develop a new generation of Li-rich electrode materials with high capacity in general. Li_2RuO_3 is a typical layered metal oxide material, which consists of transition metal layers and lithium layers, as depicted in Fig. 1 (a). Each transition metal (TM) layer is separated by a lithium layer in which oxygen forms the cubic close packing in the lattice. In the TM layer, 1/3 Li^+ and 2/3 Ru^{4+} ions occupy the 4*d* and 8*f* sites. These layers are composed out of edge-sharing RuO_6/LiO_6 octahedral that are arranged in a two-dimensional hexagonal network, in which Li ions are surrounded by six Ru ions and form the honeycomb-type [$LiRu_6$] superlattice ordering, which makes the structure more stable for reversible lithium ion extraction. Furthermore, the adjacent Ru^{4+} ions are connected to each other with Ru-Ru bonds, which realize good electronic conductivity. Most importantly, Sathiya et al. have reported that Li_2RuO_3 exhibits a working potential plateau at 3.7 V and 4.2 V, which are attributed to the oxidation of Ru^{4+} / Ru^{5+} and $2O^{2-}$ / O_2^{2-}, respectively [23]. The anion redox mechanism ensures that almost all lithium ions can participate in the electrochemical reaction and provide capacity, which is the crucial reason that makes it to be the potential competitor in the layered cathode materials. However, Li_2RuO_3 suffers from similar drawbacks as other lithium-rich materials, with the cycle retention of this material still needs to be improved [24,25]. Some research groups have consistently attempted to incorporate an electroactive element into Li-rich layered oxides to improve the electrochemical performance [26–28]. Surprisingly, electroinactive element substitution has also proven to be a promising method to improve the cycling performance.

In this paper, we choose Ti as the element to study the effect of electrochemical inactive Ti ions substituted on Li_2RuO_3 for the following reasons: (1) The Ti ion does not participate in electrochemical reactions, which is more advantageous for stabilizing the crystal structure in the process of lithium ions migration [25,29]. (2) The radius of Ti^{4+} (0.60 Å) is smaller than that of Ru^{4+} (0.62 Å), it is therefore easier to prepare more ordered solid solution materials with it. (3) In the TM layer of Li_2RuO_3, one Li^+ and six Ru^{4+} ($LiRu_6$) form a honeycomb superlattice structure. The adjacent Ru^{4+} ions are connected via Ru^{4+}-Ru^{4+} bonds. However, the lengths of Ru-Ru bonds are different due to the dimerization of Ru, which leads to the transition of material from metal to insulating state when lowering the temperature [30,31]. The substitution of Ti may alleviate the dimerization of Ru-Ru bonds and therefore optimize electronic conductivity and improve the electrochemical performance. Sathiya et al. have reported the effect of electroinactive Sn^{4+} and Ti^{4+} substitution of Li_2RuO_3 on the structural and electrochemical properties. They proved that both Sn^{4+} and Ti^{4+} could help enhance the cyclability and reduce voltage decay [23,29]. Abdul et al, revealed that Ti substitution favored superior structural stability and could improve the electronic conductivity by comparing $Li_2Ru_{0.75}Ti_{0.25}O_3$ and $Li_2Ru_{0.75}Sn_{0.25}O_3$ [25]. Nevertheless, it is not sufficient only to use XRD for structural characterization that is not capable to detect very subtle changes induced by the elemental substitution. The slight structural differences, especially the arrangement of Li owing to the low electronic density cannot be detected by X-ray diffraction directly [32]. Li solid-state nuclear magnetic resonance (NMR) spectroscopy is a very sensitive tool for studying the local structure around the lithium, especially for materials with chemical disorders that cannot be easily characterized by diffraction methods that are more sensitive for long range correlations [33–35]. Therefore, for the first time, NMR was used to investigate the effect of Ru substitution by electrochemical inactive Ti ions on the structure and consequently on the electrochemical properties. The results of this study may also provide a theoretical foundation for the development and design of the next generation of high performance electrode materials.

2. Experimental

All syntheses of $Li_2Ru_{1-x}Ti_xO_3$ compounds were carried out by conventional solid-state reactions, using proper amounts of Li_2CO_3 (Aldrich 99%), RuO_2 (Aldrich 99.9%) and TiO_2 (Aldrich > 99.5%). The starting materials were mixed using ethanol in an agate mortar for two hours and pressed into a pellet. After being sintered at 950 ℃ for 24 hours in an alumina crucible with heating rate of 5 K min^{-1} followed by the rate of 4 K min^{-1} cooling down to room temperature in the air, the resulting powder of $Li_2Ru_{1-x}Ti_xO_3$ compounds were acquired. Powder Synchrotron X-ray diffraction patterns (SXRD) for $Li_2Ru_{1-x}Ti_xO_3$ (x = 0, 0.2, 0.4, 0.6, 0.8) were performed at High Resolution Powder Diffraction beamline (P02.1) at PETRA-III, DESY, Hamburg with collaboration of PETRA staff (λ = 0.207170 Å). A Laboratory X-ray diffraction (XRD) pattern for Li_2TiO_3 was recorded with a Rigaku AXS D8 diffractometer with Cu-$K\alpha$ radiation. The morphology of the materials was studied with a JSM-6700F scanning electron microscope (SEM) with an accelerating voltage of 20 kV. The electrochemical properties of the pre-

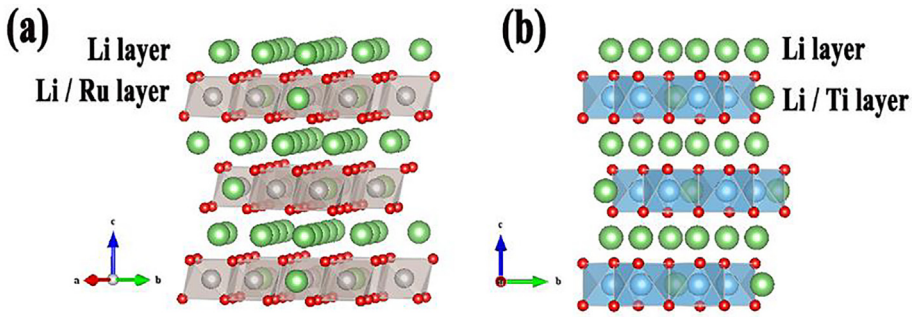

Fig. 1. Schematic crystal structure of (a) Li_2RuO_3 and (b) Li_2TiO_3.

pared $Li_2Ru_{1-x}Ti_xO_3$ compounds were examined by assembling coin-type half cells with lithium foil as the counter electrodes. The working electrodes were prepared by mixing the $Li_2Ru_{1-x}Ti_xO_3$ active materials, Super-P conductive and the polyvinylidene fluoride (PVDF) binder in N-methylpyrrolidone (NMP) in a weight ratio of 7:2:1 and coated on an Al foil current conductor. The electrode films were dried in a vacuum oven at 120 ℃ for 10 hours in succession. After dividing the electrode film into a 0.8 × 0.8 cm^2 square, the coin cells were assembled in a glove box full of Ar ($O_2 \leq 0.1$ ppm, $H_2O \leq 0.1$ ppm). The electrodes were separated by a Celgard 2400 polymer membrane. The electrolyte was a 1 mol L^{-1} lithium hexafluorophosphate ($LiPF_6$) dissolved in ethylene carbonate (EC), dimethyl carbonate (DMC), and ethyl methyl carbonate (EMC) with EC:DMC:EMC = 1:1:8 (v:v). Galvanostatic charge/discharge cycling was performed between 2.0 and 4.5 V at a current density of 20 mA g^{-1} on a Land (Wuhan, China) automatic battery tester. Cyclic voltammetry (CV) and electrochemical impedance spectroscopy (EIS) were performed on a VSP multichannel potentiostatic–galvanostatic system (Bio-Logic SAS, France). The scan rate of CV is 0.05 mv s^{-1}. The EIS data were recorded at OCV in advance of the formation procedure by applying an AC voltage amplitude of 5 mV in the frequency range from 1 MHz to 1 mHz.

Magnetization vs. temperature was measured with Vibrating Sample Magnetometer option (VSM) installed in the Physical Property Measurement System (PPMS) device from Quantum Design from 2 K to 300 K. The sample has been first cooled down from room temperature to 2 K in zero field (ZFC) and then the magnetization has been measured during heating in settle mode at a magnetic field of 10 kOe ($\mu_0 H$ = 1 T) before the sample was again cooled down in field (FC) to measure again during heating. For ^{7}Li magic-angle spinning (MAS) NMR, a Bruker Avance 200 MHz spectrometer (4.7 T) with 1.3 mm zirconia rotors and a spinning frequency of 60 kHz was used. The experiments were performed with a rotor synchronized Hahn-echo pulse sequence ($\pi/2 - \tau - \pi - \tau$-acquisition), a $\pi/2$ pulse length of 0.6 μs, and a recycle delay of 0.25 s at a frequency of 77.78 MHz. All spectra were acquired at room temperature without further cooling of the probe. An aqueous 1 M LiCl solution was used as the reference for the chemical shift of ^{7}Li (0 ppm). All spectra were normalized according to the number of scans and the sample mass.

3. Results and discussion

The schematic crystal structure of Li_2TiO_3 is shown in Fig. 1(b), the structure of Li_2TiO_3 is similar to that of Li_2RuO_3. They crystallize in the same space group ($C2/c$) and both are made of lithium layers and TM layers forming honeycombs. The only difference is that in the TM layer of Li_2RuO_3 Ru ions occupy 8*f* position, however, Ti ions in the TM layer occupy 4*e* position.

The layered $Li_2Ru_{1-x}Ti_xO_3$ (x = 0, 0.2, 0.4, 0.6, 0.8, 1) series cathodes were synthesized through high-temperature reaction and the single phase solid solution character has been confirmed by evaluation of SXRD patterns with high intrinsic resolution (the end member Li_2TiO_3 has been measured using a laboratory Rigaku AXS D8 diffractometer with Cu Ka radiation due to a technical problem that occurred for that sample during the synchrotron measurement). The X-ray diffraction patterns are further analyzed using Rietveld refinement, as shown in Fig. 2. Considering the atomic exchange, we permit both Ti and Ru ions change occupation with the Li ions in the TM layer and Li layer equally in the refined structural model. The good agreement of the calculated curves with the experimental patterns, and the reasonable R_{wp} values (listed in Table S1) reveal that our structural model is suitable for accounting the structural evolution of the series with Ti substitution. Here we only take $Li_2Ru_{0.8}Ti_{0.2}O_3$ as an example, the refinement result is shown in Table S2, the occupancy of Ti ions that occupy the TM site (8*f*, Wyckoff site) is 17.5(5)%, which means that small number of Ti ions exchange position with adjacent Li ions in the TM-layer and even the Li ions in the Li layer. It's worth noting that the ion exchange rate increase with the increasing amount of substitution Ti atoms. When x = 0.4, 0.6, 0.8 and 1, the mixing ratio of transition metal and lithium ions are 7.8(5)%, 8.1(2)%, 8.4(3)%, and 8.7(1)%, respectively. This phenomenon has been reported in the other literature that Ti substitution could increase the mobility of ions. The role of Ti ions in the Li-layer will be discussed in the NMR part in detail. For Li_2RuO_3, the five reflections between 2.6° and 4.5° represent the [$LiRu_6$] honeycomb structure in the TM layer. However, the superstructure reflections become less intense with the increase of Ti. The enlarged XRD patterns are shown in Fig. S1. When x = 0.8, the superstructure reflections are almost impossible to observe owing to the increased ion exchange and number of stacking faults. The inset of Fig. S1 exemplarily shows the continuous shift to higher scattering angles of the 003 reflection (directly correlated with the c lattice parameter evolution) with incremental substitution of Ru with Ti clearly indicating the existence of a solid solution for the $Li_2Ru_{1-x}Ti_xO_3$ series. The unit-cell lattice parameters obtained from Rietveld refinement are shown in Fig. S2, the almost linear evolving lattice parameter c with increasing Ti substitution is a strong proof for the existence of a solid solution series of $Li_2Ru_{1-x}Ti_xO_3$. The decrease of the interlayer spacing as reflected by lattice parameter c can easily be explained by the smaller ionic radius of Ti^{4+} compared with Ru^{4+}. On the contrary, the values of lattice parameter a and b expand with more Ti substitution, which is a common observation consistent with descriptions in literature [29,36]. The expansion of parameter a and b could help to stabilize the crystal structure by improving the integrity of the Li_2MO_3 structures and facilitates electron transport and Li^+ diffusion kinetics.

The SEM pictures of the synthesized $Li_2Ru_{1-x}Ti_xO_3$ (x = 0, 0.2, 0.4, 0.6, 0.8, 1) cathodes are depicted in Fig. S3. The particle morphology is polyhedral with a particle size of hundreds of nanometers and a smooth surface. The substitution of Ti has only little effect on the morphology.

The electrochemical properties were tested between 2.0 and 4.5 V at a current density of 20 mA g^{-1} and the first charge–discharge profiles are compared in Fig. 3. Because Li_2TiO_3 does not show any electrochemical activity in this voltage range, therefore, the x = 1 case is not considered in the electrochemical tests. The first charge capacity of Li_2RuO_3 is 313 mAh g^{-1}, which is very close to the theoretical capacity (328 mAh g^{-1}), and corresponds to a 1.9 Li^+ extraction per formula unit from the cathode material. The first discharge capacity could still reach 307 mAh g^{-1}. Therefore, the initial coulomb efficiency is 98%, higher than traditional x $Li_2MnO_3 \cdot (1\text{-}x)$ $LiMeO_2$ (Me = Ni, Co, Mn, Fe, etc.) compounds (about 75%). In the initial charge process, Li_2RuO_3 exhibits a working potential plateau at around 3.7 V and 4.2 V, respectively, which could be attributed to the oxidation of Ru^{4+} / Ru^{5+} and $2O^{2-}$ / O_2^{2-} as reported in other researches [22,23,29]. This anion redox process is the main reason for the high initial coulomb efficiency of Li_2RuO_3. The discharge profile is composed of a slope region without any obvious plateaus. When increasing the Ti content, as expected, the working potential plateau at 3.7 V becomes shorter and shorter due to the decrease of electrochemical active Ru ions. However, the plateau at 4.2 V displays a completely opposite change.

When x = 0, 0.2, 0.4, 0.6 and 0.8, the specific capacities contributed to this platform region are 130, 166, 187, 193 and 133 mAh g^{-1}, respectively. According to the other literature, a small amount of Ti substitution can promote the changes in the valence of oxygen elements or oxygen release [25,29,36]. On the other hand, the first coulomb efficiency of this series compounds are

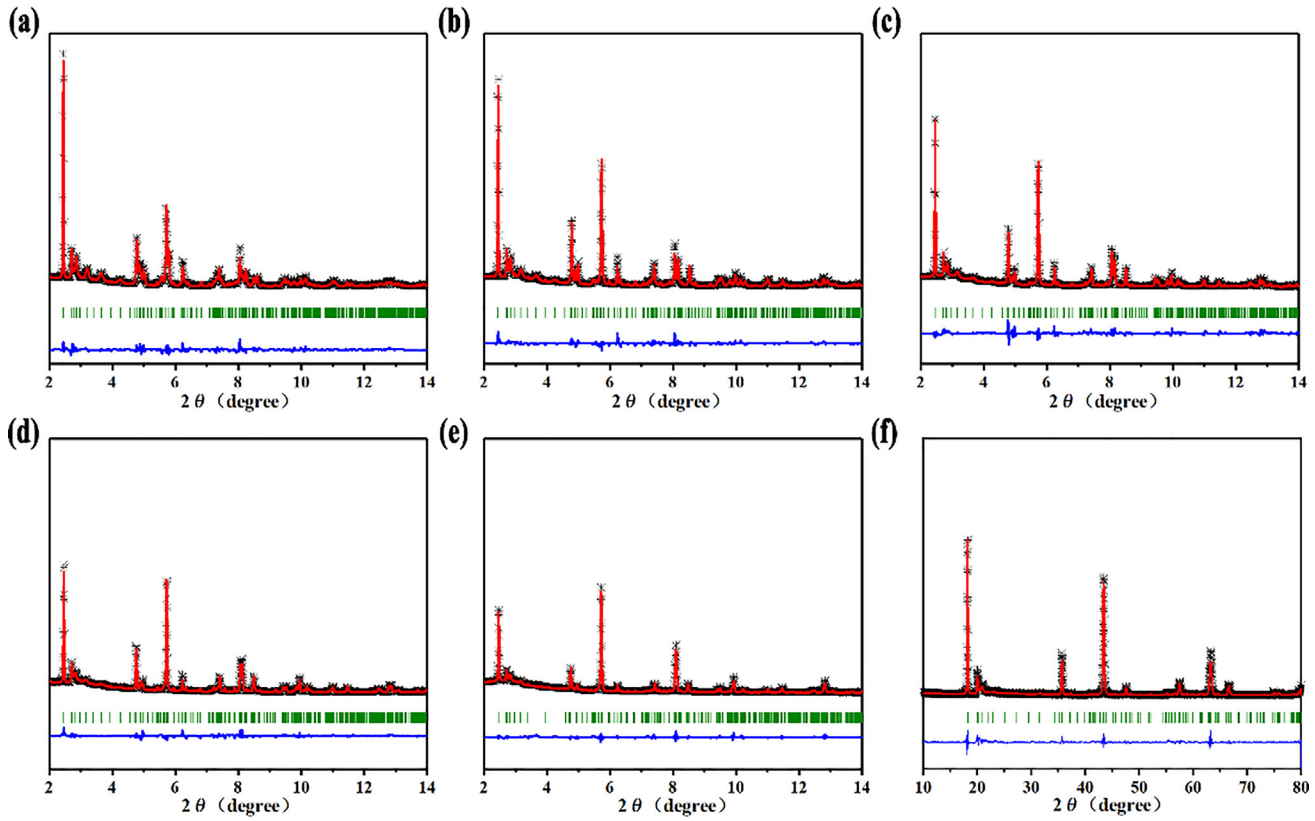

Fig. 2. Refinement results for (a)-(e) $Li_2Ru_{1-x}Ti_xO_3$ (x = 0, 0.2, 0.4, 0.6, 0.8) obtained from synchrotron radiation diffraction (SXRD) and for (f) Li_2TiO_3 obtained from laboratory XRD. Black crosses, red and blue lines represent the observed, calculated, and difference patterns, respectively. Green vertical ticks mark Bragg positions corresponding to the *C*2/*c* space group.

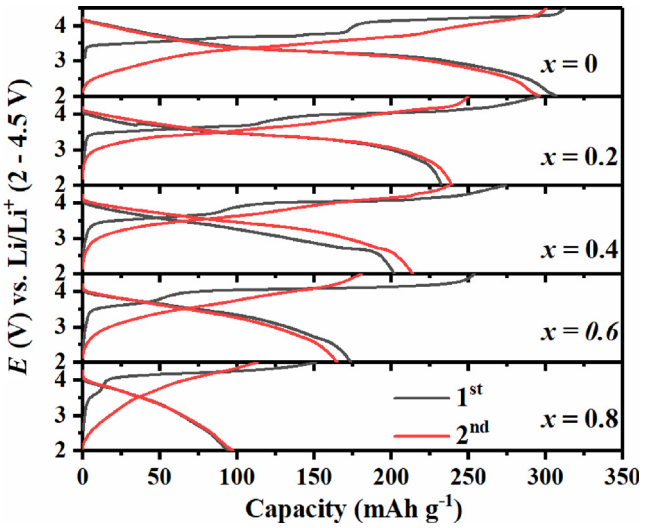

Fig. 3. The first and second charge/discharge curves of $Li_2Ru_{1-x}Ti_xO_3$ (x = 0, 0.2, 0.4, 0.6, 0.8) samples between 2.0 and 4.5 V vs. Li/Li^+ at a current density of 20 mA g^{-1}

98%, 77%, 73%, 71% and 60%, respectively, which can also prove our conjecture that oxygen loss becomes more serious with the increase of Ti ions. The Ru (4*d*)-O (2*p*) band overlap is larger than that of Ti (3*d*)-O (2*p*), therefore the covalent character of the Ru-O band is stronger [25]. These structural and electronic features of Ti-substituted samples limit the 'flexibility' of the oxygen lattice, which is therefore more prone to O_2 release [20].

The second charge profiles of the five samples show much difference with the first one. It's very hard to distinguish the two platforms in the charging process, which indicate that there should be an irreversible structural transformation during the first charging process.

The corresponding cyclic voltammetry tests at a scanning rate of 0.05 mv s^{-1} are shown in Fig. S4. With the decreasing amount of Ru, the oxidation peak at 3.7 V related to the change in the valence of Ru^{4+} decreases gradually. On the contrary, the oxidation peak of the oxygen element over 4.2 V does not decrease with the increasing amount of Ti, what coincides well with the charge–discharge profiles.

The electrochemical cycle stability of the solid solution series is compared in Fig. 4. Interesting to find that the discharge capacity of $Li_2Ru_{0.2}Ti_{0.8}O_3$ compound could stable over 100 mAh g^{-1}, which exceeds the theoretical capacity (65 mAh g^{-1}). Ti substitution will promote the formation of O_2^{n-} species based on the other literature [25,29,36], therefore extra capacity can be linked to the reversible redox activity of oxygen. Even though the introduction of Ti ions leads to the loss of specific capacity due to the electrochemical inactivity of Ti ions. The electrochemical cycle stability is improved with the increase of Ti ions. After 50 cycles, the discharge-specific capacity cycle retentions are 81%, 90%, 85% and 84%, respectively. As for x = 0.8, the stable capacity after 50 cycles is even higher than that of the first cycle. A significant increase in cyclic stability can also be observed from the rate performance (Fig. S5).

In addition, to investigating the influence of Ti substitution on the conductivity of materials, EIS in open circuit states are measured as shown in Fig. 5. The impedance spectrum is fitted with the model given in Fig. S6. As seen in the figure, an intercept at

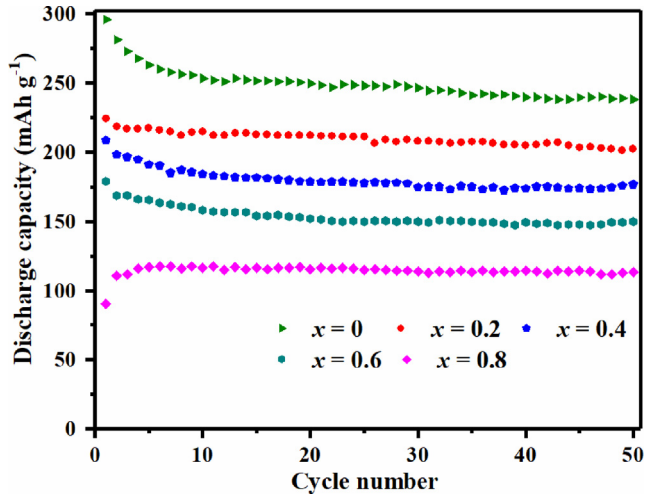

Fig. 4. Discharge capacity retention of $Li_2Ru_{1-x}Ti_xO_3$ (x = 0, 0.2, 0.4, 0.6, 0.8) samples.

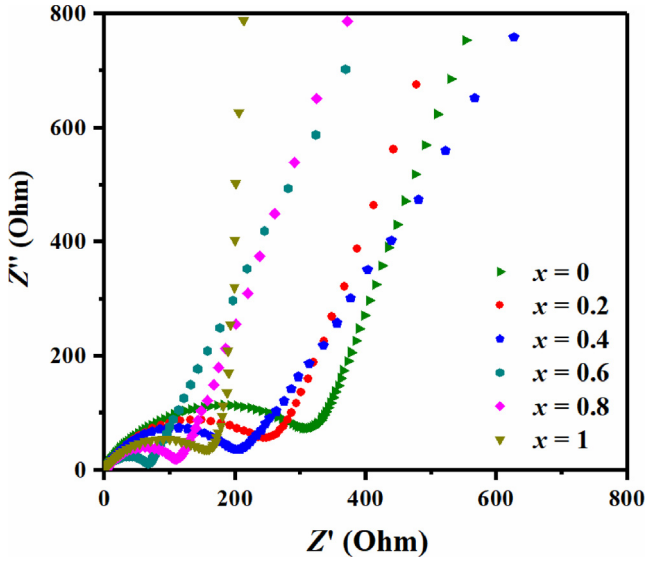

Fig. 5. The Nyquist plots of $Li_2Ru_{1-x}Ti_xO_3$ (x = 0, 0.2, 0.4, 0.6, 0.8, 1).

the Z' axis in high frequency corresponds to the ohmic resistance (R_s) of the battery, which includes the resistance of the electrolyte, separator, electrode, etc. The depressed semicircle in the middle frequency range is attributed to the charge transfer resistance (R_{ct}) and the double layer capacitance (CPE). The inclined line in the low frequency region represents the Warburg impedance (W_o), which is associated with the Li^+ ion diffusion. The test results show that there is only one semicircle in the open circuit state, which presents charge transfer resistance in the open circuit state. The fitting results that are shown in Fig. S7. R_s and R_{ct} obtained from the fitting results are listed in Table 1, it is obvious that when the amount of Ti ions is less than 0.6, the charge transfer resistance decreases with the increase of Ti content. Electronegativity is a measure of the tendency of an atom to attract a shared pair of electrons respectively electron density and is an important factor that plays a role concerning the electrochemical potential of electrodes. A large difference in electronegativity of the constituents usually results in the formation of a more ionic bond. Strong electronegative elements usually can gain more electron transfers from lithium atoms, forming a stronger ionic bond [37]. The Pauling values of electronegativity for Ru, Ti and O is 2.20, 1.54 and 3.44, respectively [25]. Therefore, the bonding between the transition metal and oxygen is 1.24 (Ru-O) and 1.90 (Ti-O). Hence, the larger electronegativity Ti-O could improve conductivity, because Ti ions has a stronger interaction with the adjacent O^{2-} anions. However, too much titanium (x = 0.8, 1) will be counterproductive due to its nature as electronic insulator.

Table 1
Equivalent circuit parameters of $Li_2Ru_{1-x}Ti_xO_3$ (x = 0, 0.2, 0.4, 0.6, 0.8, 1) obtained from fitting the experimental impedance spectra.

	R_s (Ω)	R_{ct} (Ω)
x = 0	1.567	331.3
x = 0.2	1.586	274.7
x = 0.4	1.353	219.1
x = 0.6	1.505	73.1
x = 0.8	2.758	120.9
x = 1	1.757	172.4

The inclined line in the low frequency region represents the Warburg impedance, which is associated with the Li^+ ion diffusion. The apparent diffusion coefficient of Li^+, D_{Li}, can be calculated by the equation [38]

$$D_{Li} = \frac{0.5R^2T^2}{S^2n^4F^4C^2\sigma^2}$$

In this equation, R is the gas constant, T the absolute temperature, F the Faraday constant; and σ is the Warburg factor which obeys the following relationship:

$$Z' = R_S + R_{CT} + \sigma\omega^{-1/2}$$

Fig. S8 displays the linear fitting of Z' vs. $\omega^{-1/2}$, from which the slope σ can be obtained. The lithium diffusion coefficients of $Li_2Ru_{1-x}Ti_xO_3$ are listed in Table S3. The substitution of Ti ions can promote the diffusion of Li ions, however, when the Ti content reaches x = 0.6 the Li diffusion coefficient reaches its maximum. Li diffusion coefficient decreases with more Ti substitution, which may relate to the smaller interlayer spacing.

The magnetic susceptibility as a function of temperature is shown in Fig. S9 (a). The ZFC and FC branch of all samples overlap to large extend until lowest temperatures indicating that there is no transition from paramagnetic to ferro-/ferrimagnetism down to 2 K (therefore only the FC branches are shown in the figures). From the linear region of the inverse susceptibility vs. temperature the effective magnetic moments as a function of temperature have been derived and is presented in Fig. S9 (b). Ti^{4+} has electronic configuration [Ar] $4s^0$ $3d^0$ without any unpaired electrons and in agreement Li_2TiO_3 has zero effective magnetic moment. In Li_2RuO_3 Ru^{4+} has the electronic configuration [Kr] $5s^0$ $4d^4$ with two unpaired electrons (total spin S = 1) in octahedral coordination in low-spin state (t_{2g}:4) that bear a theoretical effective spin-only moment of μ_{eff} = 2.8 μ_B. However, the experimentally observed effective magnetic moment for Ru^{4+} in Li_2RuO_3 is somewhat lower at only 2.28(1) μ_B at 300 K, but this in good agreement with observation presented in literature [39]. It is a result from the Ru-Ru partial bonding that affects (decreases) the number of effective unpaired electrons. Interestingly, the effective magnetic moments of the solid solution series $Li_2Ru_{1-x}Ti_xO_3$ do not exhibit a linear dependence with Ti substitution x in contrast to the evolution of the lattice parameters. This reveals the strong non-linearity of Ru-Ru bonding and total effective spin of the solid solution series even though the unit cell parameters exhibit these linearities.

It is well known that nuclear magnetic resonance (NMR) measurements are useful for further study of the chemical environment in which atoms are located, especially for the compounds with chemical disorders. Following the model of Grey et al., we account for the observed shifts in the NMR data of the family with the model for paramagnetic Fermi contact (FC) shifts for lithium

oxides containing paramagnetic metals with octahedral geometry [35,40,41]. The observed shift was contributed from all paramagnetic metal – O – Li bonds, and whether the shift is positive or negtive deponds on the bond angle and the electronic configuration. For example, in our case, because titanium (IV) does not contribute to a FC shift in Li_2TiO_3 and hence in the whole $Li_2Ru_{1-x}Ti_xO_3$ series, the number of surrounding Ru and their positions therefore control the FC shift of the Li atoms. As shown in Fig. 6 (a), Li^+ ions (green) are located in an oxygen octahedron surrounded by Li, Ru or Ti atoms. In the Li layer, one Li^+ can form eight 90° Ru – O – Li (Ru_{90}) bonds and four 180° Ru – O – Li (Ru_{180}) bonds. In the TM layer, Li ions are surronded by six Ru_{90} (honeycomb structure). According to the model proposed by Grey et al., 90° Ru – O – Li bonds contribute to a positive FC shift through delocalization and the 180° Ru – O – Li bonds generate a negative FC shift on the Li by a polarization mechanism. Therefore, according to this model, the Li^+ ions in the TM layer can be assigned to high shift values, whereas the Li ions in the Li layer are represented by low shift values. .

The ^{7}Li MAS NMR test results of $Li_2Ru_{1-x}Ti_xO_3$ are shown in Fig. 6 (b). The ^{7}Li MAS NMR test of Li_2TiO_3 presents typical insulator characteristics, and only a sharp peak is detected at around 0 ppm. The ^{7}Li NMR test of Li_2RuO_3 is completely different from that of Li_2TiO_3, and clearly shows a paramagnetic character of the local Li environment. Based on the sturctural model, one would expect two clearly distiguishable Li enviroments at about 40 ppm (Li in Li layer, 4 Ru_{90} + 4 Ru_{180}) and 400 ppm (Li in TM layer, 6 Ru_{90}). (Shifts are based on the values used in the paper from Elodie Salager 2014) [32]. However, additional signals at 200 (3 Ru_{90}) and 550 ppm as well as a significant peak broadening can be observed. This can be assigned to a rather pronounced local disorder (Ru-dimers, stacking faults, etc). With the substitution of Ru with Ti,

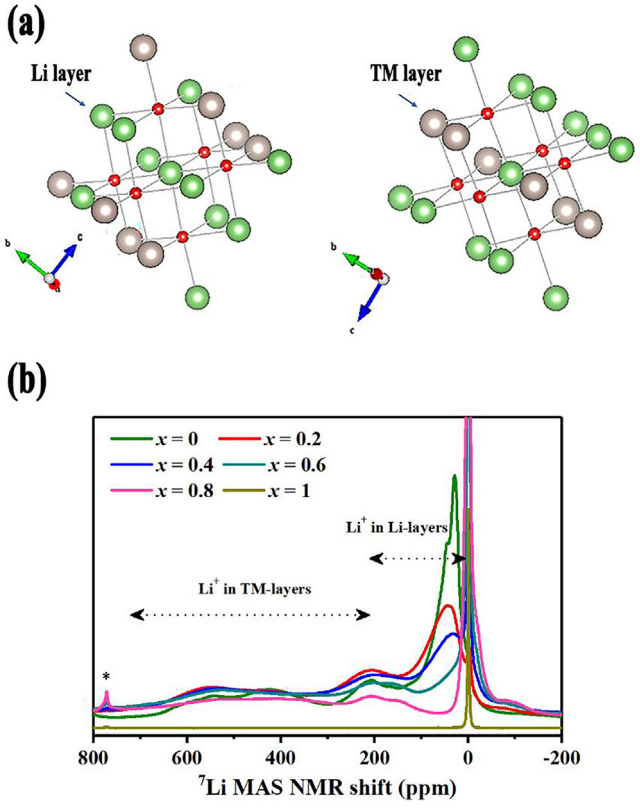

Fig. 6. (a) Environment for Li^+ in Li layers and for Li in TM layers in Li_2RuO_3. Ru are in shiny gray, Li are in green and oxygens are in red; (b) ^{7}Li MAS NMR spectra of $Li_2Ru_{1-x}Ti_xO_3$, the MAS spinning sideband at around 780 ppm (marked with *) is caused by the rotation of the sample in the NMR magnet.

the following changes can be observed: At −110 ppm: For x = 0.2, a broad signal at around −80 ppm arises and increases in intensity for higher Ti/Ru ratios. The signal can be attributed to Li in the Li layer with a mixed Ti/Ru enviroment and at least one Ru_{180} bond (negative contribution). The signal rise in signal intensity is well in agreement with thinning of the Ru content. At 0 ppm: For x = 0.2 a rather narrow signal at around 0 ppm arises and increases in intensity for higher Ti/Ru ratios. Furthermore, for higher Ti/Ru ratios the peak broadens steadily. The peak represents local Li environments, both Li and Ru layer, with a strong diamagnetic character as observed in pure Li_2TiO_3. However, a contribition from mixed Ti/Ru enviroments might further increase the signal intensity. At 40 ppm: The broad signal at 40 ppm decreases in intensity for higher Ti/Ru ratios. This observation is well in agreement with a gradual substituion of Ru with Ti in the local enviroment of Li in the Li layer. The decrease in signal intensity matches well with the increase at around 0 ppm and −80 ppm, respectively. At 200–600 ppm: With Ti substitution the signals at high shift values are more broadened and exhibit a higher signal intensity at about 550 and 200 pm in comparison to pure Li_2RuO_3. Very interestingely, the signals at 400 and 550 ppm for x = 0.2 to x = 0.6 do not decrease in intensity.

The peak represents lithium ions in TM layer at 200 ppm (3 Ru_{90}) and 400 ppm (6 Ru_{90}) becomes less intense with the increased amount of Ti ions, which indicates that the superlattice structure disappears gradually. This is consistent with the refinemnent results of XRD measurement.

Since the initial charge capacity of Li_2RuO_3 exceeds 300 mAh g^{-1}, almost all Li^+ ions will be removed from the lattice during the first charge process. Even though the long-range order of the layered structure is maintained, there will be a large lattice distortion. When part of the Ti ions is embedded in the Li layer, although it does not take part in electrochemical reaction, Ti ions could help to keep the layered structure from collapsing on the condition that all the lithium ions are removed, and sufficient space is provided for the re-insertion of Li^+ ions to improve cycle stability.

4. Conclusions

In summary, $Li_2Ru_{1-x}Ti_xO_3$ (x = 0, 0.2, 0.4, 0.6, 0.8, 1) solid solution were successfully synthesized by high-temperature reaction. The effect of electrochemically inactive Ti substitution can be summarized in two aspects: structure and electrochemical performance. Both of the refinement result of X-ray diffraction and NMR verify that some Ti ions go to the position of Li ions in the Li and TM layer, which help keep the layered structure from collapsing while Li^+ inserting/de-intercalating during the electrochemical process. The electrochemical test results reveal that Ti ions substitution could promote a change in the valence of oxygen during the first charge process and improve the stability of long cycles. Even though the substitution of electrochemical inactive Ti cause the decrease of capacity, however, the electrochemical impedance spectra exhibits the positive influence of Ti substitution: resisting the charge transfer impedance, which facilitates better Li-ion diffusion and improved electronic conductivity. Therefore, the quantity seems like very important for electrochemical inactive element substitution.

Declaration of Competing Interest

The authors declare that they have no known competing financial interests or personal relationships that could have appeared to influence the work reported in this paper.

Acknowledgements

This work was supported by the Nature Science Foundation of Changchun Normal University and Research Foundation for Advanced Doctor of Changchun Normal University. This work contributes to the research performed at CELEST (Center for Electrochemical Energy Storage Ulm-Karlsruhe).

Appendix A. Supplementary data

Supplementary data to this article can be found online at https://doi.org/10.1016/j.jechem.2020.12.037.

References

[1] B. Scrosati, J. Garche, J. Power Sources 195 (2010) 2419–2430.
[2] V. Etacheri, R. Marom, R. Elazari, G. Salitra, D. Aurbach, Energy Environ. Sci. 4 (2011) 3243.
[3] P. He, H. Yu, D. Li, H. Zhou, J. Mater. Chem. 22 (2012) 3680.
[4] C. Zhao, Q. Wang, Y. Lu, Y.-S. Hu, B. Li, L. Chen, J. Phys. D 50 (2017) 183001.
[5] Y.-X. Yao, C. Yan, Q. Zhang, ChemComm 56 (2020) 14570–14584.
[6] R. Zhang, Z. Xue, J. Qin, M. Sawangphruk, X. Zhang, R. Liu, J. Energy Chem. 50 (2020) 143–153.
[7] R. Wang, Y. Sun, K. Yang, J. Zheng, Y. Li, Z. Qian, Z. He, S. Zhong, J. Energy Chem. 50 (2020) 271–279.
[8] Y. Wang, F. Yu, J. Alloys Compd. 850 (2021) 156773.
[9] J. Li, M. Zhang, D. Zhang, Y. Yan, Z. Li, Chem. Eng. J. 402 (2020) 126195.
[10] J.R. Dahn, T. Zheng, Y. Liu, J.S. Xue, Science 270 (1995) 590–593.
[11] N.A. Kaskhedikar, J. Maier, Adv. Mater. 21 (2009) 2664–2680.
[12] M. Winter, J.O. Besenhard, M.E. Spahr, P. Novak, Adv. Mater. 10 (1998) 725–768.
[13] S.-K. Hu, G.-H. Cheng, M.-Y. Cheng, B.-J. Hwang, R. Santhanam, J. Power Sources 188 (2009) 564–569.
[14] H. Zheng, Q. Sun, G. Liu, X. Song, V.S. Battaglia, J. Power Sources 207 (2012) 134–140.
[15] B.J. Hwang, Y.W. Tsai, D. Carlier, G. Ceder, Chem. Mater. 15 (2003) 3676–3682.
[16] V.R. Chitturi, L.M.R. Arava, I. Yasuyuki, A. Pulickel, ACS Appl. Mater. Interfaces 3 (2011) 2966–2972.
[17] Y. Li, Y.-S. Hu, X. Qi, X. Rong, H. Li, X. Huang, L. Chen, Energy Storage Mater. 5 (2016) 191–197.
[18] Y. Li, Y. Lu, C. Zhao, Y.-S. Hu, M.-M. Titirici, H. Li, X. Huang, L. Chen, Energy Storage Mater. 7 (2017) 130–151.
[19] J. Lee, A. Urban, X. Li, D. Su, G. Hautier, G. Ceder, Science 343 (2014) 519–522.
[20] B. Li, R. Shao, H. Yan, L. An, B. Zhang, H. Wei, J. Ma, D. Xia, X. Han, Adv. Funct. Mater. 26 (2016) 1330–1337.
[21] S. Taminato, M. Hirayama, K. Suzuki, K. Kim, Y. Zheng, K. Tamura, J.i. Mizuki, R. Kanno, J. Mater. Chem. A 2 (2014) 17875–17882.
[22] M. Sathiya, K. Ramesha, G. Rousse, D. Foix, D. Gonbeau, A.S. Prakash, M.L. Doublet, K. Hemalatha, J.M. Tarascon, Chem. Mater. 25 (2013) 1121–1131.
[23] M. Sathiya, G. Rousse, K. Ramesha, C.P. Laisa, H. Vezin, M.T. Sougrati, M.L. Doublet, D. Foix, D. Gonbeau, W. Walker, A.S. Prakash, M. Ben Hassine, L. Dupont, J.M. Tarascon, Nat. Mater. 12 (2013) 827–835.
[24] P. Arunkumar, W.J. Jeong, S. Won, W.B. Im, J. Power Sources 324 (2016) 428–438.
[25] A.K. Kalathil, P. Arunkumar, D.H. Kim, J.W. Lee, W.B. Im, ACS Appl. Mater. Interfaces 7 (2015) 7118–7128.
[26] B. Song, C. Zhou, H. Wang, H. Liu, Z. Liu, M.O. Lai, L. Lu, J. Electrochem. Soc. 161 (2014) A1723–A1730.
[27] B. Song, M.O. Lai, L. Lu, Electrochim. Acta 80 (2012) 187–195.
[28] C. Lu, S. Yang, H. Wu, Y. Zhang, X. Yang, T. Liang, Electrochim. Acta 209 (2016) 448–455.
[29] M. Sathiya, A.M. Abakumov, D. Foix, G. Rousse, K. Ramesha, M. Saubanere, M.L. Doublet, H. Vezin, C.P. Laisa, A.S. Prakash, D. Gonbeau, G. VanTendeloo, J.M. Tarascon, Nat. Mater. 14 (2015) 230–238.
[30] S.A.J. Kimber, I.I. Mazin, J. Shen, H.O. Jeschke, S.V. Streltsov, D.N. Argyriou, R. Valentí, D.I. Khomskii, Phys. Rev. B 89 (2014) 081408.
[31] Y. Miura, Y. Yasui, M. Sato, N. Igawa, K. Kakurai, J. Phys. Soc. Japan 76 (2007) 033705.
[32] E. Salager, V. Saroukanian, M. Sathiya, M. Tang, J.B. Leriche, P. Melin, Z. Wang, H. Vezin, C. Bessada, M. Deschamps, Chem. Mater. 26 (2014) 7009–7019.
[33] P. Mustarelli, V. Massarotti, M. Bini, D. Capsoni, Phys. Rev. B 55 (1997) 73752–12024.
[34] C. Marichal, J. Hirschinger, P. Granger, M. Menetrier, A. Rougier, C. Delmas, Inorg. Chem. 34 (1995) 1773–1778.
[35] C.P. Grey, N. Dupré, Chem. Rev. 104 (2004) 4493–4512.
[36] H. Zhao, Y. Shi, L. Xue, Y. Cheng, Z. Hu, X. Liu, J. Energy Chem. 33 (2019) 9–16.
[37] D. Zhou, C. Li, F. Yin, X. Tang, C. Pu, C. He, Chin Chem. Lett. 31 (2020) 2325–2329.
[38] W. Shen, H. Li, C. Wang, Z. Li, Q. Xu, H. Liu, Y. Wang, J. Mater. Chem. A 3 (2015) 15190–15201.
[39] J.C. Wang, J. Terzic, T.F. Qi, F. Ye, S.J. Yuan, S. Aswartham, S.V. Streltsov, D.I. Khomskii, R.K. Kaul, G. Cao, Phys. Rev. B 90 (2014) 1611101–1611106.
[40] L.S. Cahill, S.C. Yin, A. Samoson, I. Heinmaa, a.L.F. Nazar, G.R. Goward, Chem. Mater. 17 (2005) 6560–6566.
[41] H. Koga, L. Croguennec, P. Mannessiez, M. Ménétrier, F. Weill, L. Bourgeois, M. Duttine, E. Suard, C. Delmas, J. Phys. Chem. C 116 (2012) 13497–13506.